Dziadosz M, Bogner W, Kreis R. Non-water-excitation MR spectroscopy techniques to explore exchanging protons in human brain at 3 T. Magn Reson Med. 2020;

Non-water-excitation MR spectroscopy techniques to explore exchanging protons in human brain at 3 T

M. Dziadosz [1,2], W.Bogner[3] and R. Kreis[1]

[1] Departments of Radiology and Biomedical Research, University of Bern, Bern, Switzerland,

[2]Graduate School for Cellular and Biomedical Sciences, University of Bern, Bern, Switzerland

[3]High-field MR Center, Department of Biomedical Imaging and Image-guided Therapy, Medical University Vienna, Vienna, Austria

Corresponding author:

Prof. Dr. sc. nat. Roland Kreis,

MR Methodology, University Bern,

Freiburgstr. 3,

CH-3010 Bern, Switzerland

Tel: +41-31-632 8174

Email: roland.kreis@insel.ch

 Published version to be found at: https://doi.org/10.1002/mrm.28322

Abstract

Purpose

To develop localization sequences for in vivo MR spectroscopy on clinical scanners of 3 T to record spectra that are not influenced by magnetization transfer from water.

Methods

ISIS localization and chemical-shift-selective excitation (termed I-CSE) was combined in two ways: first, full ISIS localization plus a frequency-selective spin-echo and second, 2-dimensional ISIS plus a frequency-selective excitation and slice-selective refocusing. The techniques were evaluated at 3 T in phantoms and human subjects in comparison to standard techniques with water presaturation or metabolite-cycling. ISIS included GOIA-type adiabatic inversion pulses; echo times were 8-10 ms.

Results

The novel 2D and 3D I-CSE methods yield upfield spectra that are comparable to those from standard MRS, except for shorter echo times and a limited frequency range. On the downfield/high-frequency side, they yield much more signal for exchangeable protons when compared to MRS with water presaturation or metabolite-cycling and longer echo times.

Conclusion

Novel non-water-excitation MRS sequences offer substantial benefits for the detection of metabolite signals that are otherwise suppressed by saturation transfer from water. Avoiding water saturation and using very short echo times allows direct observation of faster exchanging moieties than was previously possible at 3 T and additionally makes the methods less susceptible to fast T_2 relaxation.

Keywords

magnetization exchange, proton MR spectroscopy, downfield, amides, brain, human

Introduction

Standard in vivo ^{1}H Magnetic Resonance Spectroscopy (MRS) sequences include modules to suppress the otherwise overwhelmingly strong signal from water. Good water suppression (WS) ensures an easily manageable dynamic range for the receiver system and negligible baseline contributions from water in the spectral region of interest. These contributions manifest as tails from the strong water peak, but also in the form of sidebands induced by system instabilities. However, common WS techniques, which rely on magnetization saturation (e.g., CHESS (1,2) or VAPOR (3)), have also undesired side effects. They lead to attenuation of metabolite signals that are subject to direct (via proton exchange) or indirect (via cross-relaxation) magnetization transfer from water. The signal attenuation is particularly severe in the downfield/high-frequency[1] spectral range where exchangeable protons resonate. This part of the in vivo ^{1}H MR spectrum contains mainly resonances of hydroxyl, amine, amide and aromatic protons. These protons are all of low concentration and almost all of these signals are susceptible to magnetization transfer. In addition, it should be noted that fast proton exchange with water does not only cause signal attenuation when combined with water presaturation, but also, even in the absence of water presaturation, inherently leads to exchange broadening and thus short apparent transverse relaxation times.

Hence, multiple techniques without or with minimal water signal saturation have been suggested that record full intensity spectra for these exchange-affected metabolite resonances (4). Such non-water-saturation (nWS) techniques are either based on i) side band suppression (e.g. gradient-cycling (5) plus digital filtering, multi-echo acquisition (6) or real-time sideband prevention (7)); ii) selective water-signal dephasing (8,9); iii) water or metabolite signal inversion in alternate scans (10-12); or iv) non-water-excitation (nWE) techniques (5,8,13). For best sensitivity to exchangeable protons, such dedicated sequences should fulfill three criteria: i) contain no or only short time periods with magnetization disequilibrium between water and metabolite resonances within the localization/excitation sequence (e.g., no long delays after water presaturation or metabolite signal inversion); ii) have short echo time (TE); iii) feature long repetition time (TR) if the water signal is saturated/inverted or leave the water magnetization untouched in the longitudinal equilibrium state.

[1] *Chemical shifts at high frequency (with lower shielding) are historically referred to as downfield/lowfield shifts, while chemical shifts to lower frequency (greater shielding) are historically referred to as upfield/highfield shifts. This notation is maintained for consistency even though of course today's MR and high-resolution NMR scanners do not operate with variable main fields.*

 Published version to be found at: https://doi.org/10.1002/mrm.28322

These requirements are harder to fulfill at clinical field strengths (≤3 T) than at ultra-high-field (UHF) and in vivo than in vitro because frequency-selective pulses are inherently longer at low fields while B_0- and B_1-inhomogeneities are more problematic for in vivo scans than in vitro.

In recent years, the most popular nWS techniques to record downfield spectra and to study chemical exchange has been the metabolite cycling (MC) technique (10-12). MC is a two-step technique based on subtracting signals from scans in which either the upfield or downfield signals have been inverted before signal excitation. In combination with PRESS (12,14,15), STEAM (16-19), or semi-LASER (17,20), this allows for moderately short TE (10-40 ms), but always also includes relatively long periods where metabolite and water magnetization point in opposite direction (20-60 ms) and also include relatively long inversion pulses (~20 ms).

To minimize transfer of saturation, it is better to revert to nWE methods where no disequilibrium state is formed before creation of transverse metabolite magnetization. The flipback WATERGATE method is one of them—very successful in high resolution NMR, but of limited use in vivo (8). Another approach had been suggested early-on in a preliminary account (5). It consisted of combining either PRESS (21) or ISIS (22) localization with frequency-selective excitation, though only PRESS-based nWE was recommended. Later, LASER-based (23) double-echo (23,24), and triple-echo (25) methods have been optimized for the detection of nicotinamide-adenine dinucleotide (NAD^+). Furthermore, the transfer of longitudinal magnetization in the recovery period after excitation was exploited at UHF up to 21 T to obtain longitudinal relaxation enhancement (LRE) in animal experiments; based on LASER localization (13,26,27) or a spin-echo (10). Almost all of the above nWE techniques are efficiently preventing saturation transfer, but their rather long TEs lead to undesirable T_2-relaxation-related signal loss. Minimal TEs can be achieved with ISIS, which has recently been optimized for downfield resonances in rats at 9.4 T (28).

The aim of the current study is to explore new ways to detect downfield metabolite signals from exchangeable protons at the clinical field strength of 3 T. One is based on 3D ISIS and the other on 2D ISIS in combination with a frequency- and slice-selective spin echo. In addition, the results are compared with spectra obtained via MC-based nWS MRS.

 Published version to be found at: https://doi.org/10.1002/mrm.28322

2. Methods

2.1 Basic sequence design

Both proposed nWE sequences are based on ISIS localization (22), i.e. localization is based on constructive summation of recordings from multiple acquisitions with appropriately combined slice-selective adiabatic inversion pulses applied before the excitation pulse and where signals from outside the volume of interest (VOI) are cancelled by appropriate destructive interference. In OSIRIS (29), ISIS is additionally combined with outer volume suppression (OVS).

The two proposed techniques are schematically presented in Figure 1. The first method (Fig 1a) relies on three-dimensional ISIS and chemical-shift-selective excitation (termed 3D I-CSE). It corresponds to a standard ISIS sequence that uses a combination of eight different acquisitions, where the usual non-frequency-selective 90° excitation pulse was rendered frequency-selective. The excitation module was implemented as a spin echo module with two frequency-selective pulses and a pair of spoiler gradient pulses, but could be replaced by a single selective excitation pulse. The second sequence—two-dimensional ISIS localization with Chemical-shift-Selective Excitation (2D I-CSE)—is presented in Fig. 1b. In contrast to 3D I-CSE, spatial selection is achieved using a slice-selective refocusing pulse instead of an ISIS inversion module for one dimension. Thus, only two adiabatic inversion pulses precede the frequency-selective excitation, while the frequency-selective refocusing pulse from 3D I-CSE is replaced by a slice-selective 180° pulse. Since the ISIS elements select in two directions only, a combination of 4 different scans is sufficient. This method can also be seen as derived from the SPECIAL method (30), where the conversion would entail replacing the slice-selective excitation by frequency-selective excitation and extending the 1D ISIS prepulse into a second direction.

The schemes in Fig. 1 schematically also show the optional sequence elements: OVS pulses and CHESS WS to precede the nWE sequences. This CHESS module can be activated to evaluate the effects of conventional WS in standard clinical MRS.

2.2 Implementation specifics and acquisition parameters

All measurements were performed on a 3T whole-body MR system (Prisma, Siemens Healthineers, Germany) using the body coil for transmit and a 20-channel head coil as receiver.

 Published version to be found at: https://doi.org/10.1002/mrm.28322

The adiabatic inversion pulses for ISIS were implemented as gradient-modulated offset-independent adiabatic (GOIA) pulses (31,32) with WURST (16, 4) shapes (33). The ISIS cycles were played out as listed in Figure 1. Frequency-selective 90° excitation was realized by a Gaussian-weighted sinc pulse (3 ms pulse length corresponding to 290 Hz excitation bandwidth, center frequency at 9.7 ppm for 2D I-CSE and 8.7 ppm for 3D I-CSE for downfield recordings). The frequency-selective refocusing pulse in 3D I-CSE used the same basic shape (3 ms duration) and was paired with spoiler pulses along all 3 directions to suppress spurious signal pathways. A 4.8 ms Mao pulse (1250 Hz bandwidth) was used for slice-selective refocusing in 2D I-CSE (34).

Water presaturation (3 Gaussian RF pulses with 70 Hz bandwidth and 89, 83, and 161° flip angle (35)) was interleaved with 6 OVS pulses (total duration 470 ms).

Flip angles (FA) were calibrated for each VOI using the manufacturer's default B_1-mapping method. B_0-shimming was performed using FASTESTMAP.

In most examinations, data sets were acquired as average of 128 scans. For better comparability between experiments, scans were recorded in an interleaved manner (4 times 32 acquisitions each). For I-CSE, non-water-suppressed and water-suppressed upfield or downfield spectra were acquired in this interleaved manner, followed by a reference scan with the frequency-selective excitation on-resonance with water (8 acquisitions). The reference scans were extended by a presaturation module with 3 frequency-selective Gaussian RF pulses (240 Hz bandwidth, centered at 2.7 ppm) to partially suppress strong spurious upfield signals that can originate from subcutaneous lipids in case of motion-related insufficient signal-cancelation and that could interfere subsequently with eddy current correction when the reference signal is not from a single narrow resonance.

Acquisition parameters for I-CSE included TE=8.4 ms (for 3D I-CSE) and 10.2 ms (for 2D I-CSE), TR=3000 ms, 128 averages, spectral width 5000 Hz, 4096 data points, ISIS GOIA-W(16, 4) pulses of 5 ms duration (30 kHz bandwidth) (1 ms gradient ramps). This led to a total duration of the ISIS module of 14 ms for 2D I-CSE and 21 ms for 3D I-CSE, respectively.

MC-semi-LASER spectra (method implemented as described in Ref. (20)) with and without water presaturation were recorded for comparison. Acquisition parameters for MC-semi-LASER included TE=35 ms, TR=3000 ms, 128 averages, spectral width 5000 Hz, 4096 points, localization centered at 7.0 ppm.

 Published version to be found at: https://doi.org/10.1002/mrm.28322

2.3 In vitro testing

Initial experimental testing of the novel sequences was done based on upfield spectra from a spherical phantom ('braino', GE medical systems), filled with an aqueous solution of typical brain metabolites. For comparison with standard MRS sequences, the manufacturer's PRESS sequence was used with TE 30 ms.

To determine the bandwidth of the frequency-selective excitation modules, the excitation profile was probed by recording the response of the water resonance from the braino phantom when stepping the center of the excitation frequency from -10 ppm to +10 ppm in steps of 0.5 ppm. For display purposes, the recorded water signal of each spectrum was shifted by the value of the applied transmit offset. The resulting spectra were then summed and broadened in jMRUI (36) to portray the excitation profile in Figure 2.

2.4 In vivo brain measurements

Ten healthy volunteers aged 19-42 years without history of neurologic disorders participated in this study, which had been passed by the local ethics review board; written informed consent was obtained from all subjects.

The VOI was placed superior to the lateral ventricles. Voxel sizes were 50x65x20 mm^3 and 20x40x20 mm^3 for downfield and upfield measurements, respectively. While for upfield spectra the VOI consisted predominantly of white matter (WM; VOI placed in a single hemisphere), downfield spectra were recorded from both hemispheres and the voxel included substantial contributions of gray matter (GM).

2.5 Data processing

Data processing was done using jMRUI (36)and Matlab (version 8.5.0 R2015a; Math Works, Natick, MA).

I-CSE data

Initially, data from multiple coil elements were combined in the manufacturer's standard processing routine on the MR scanner for both 2D and 3D I-CSE. Since in the case of 3D I-CSE, this coil

 Published version to be found at: https://doi.org/10.1002/mrm.28322

combination algorithm did clearly not provide optimal SNR, coil combination from raw data was performed offline in Matlab. To eliminate water sidebands and other phase distortions, spectra were eddy-current-corrected with the water reference signal (acquired as described above) using jMRUI. Subsequently, spectra were Gaussian line-broadened by 3 Hz and the 4 spectra from the 4 sets of 32 averages were manually frequency aligned using the downfield N-acetylasparate (NAA) peak at 7.8 ppm. Difference spectra between I-CSE spectra with and without WS were obtained from these preprocessed spectra.

MC-semi-LASER data

In order to separate spectra from metabolites and water, MC-semi-LASER data were processed in Matlab as described in Ref (19). This includes eddy-current correction and frequency correction of single acquisitions as well as optimized calculation of difference spectra. Line–broadening, frequency-alignment, and calculation of differences was done as for I-CSE spectra.

3. Results

3.1 Sequence testing in phantoms

The bandwidths of the excitation modules of the I-CSE sequences as evaluated in phantom scans are presented in Figure 2. In spite of equal bandwidth for the RF pulses used, the usable frequency range is much narrower in the case of 3D I-CSE than for 2D I-CSE, which is expected since 3D I-CSE includes a spin echo from two selective pulses and not just one and thus suffers from cumulated signal loss in the transition bands of the pulses. For 2D I-CSE and the particular Gaussian-weighted sinc pulse, the full-width-at-half-maximum (FWHM) of the excitation was ~800 Hz (6.5 ppm), with a flat top profile of ~3.4 ppm (400 Hz). Stop band ripples show a minimum at 5 ppm off resonance, which corresponds to the water resonance frequency when the pulse is played out at 9.7 ppm.

In vitro spectra of the standard upfield region where exchange effects are not expected to have a large influence are presented in Figure 3 as obtained by the two novel methods in comparison to a spectrum recorded by conventional PRESS localization. Visually, when scaled by the water signal, the 2D I-CSE spectrum resembles the one obtained by PRESS very closely, while the 3D I-CSE spectrum clearly mirrors the narrow sensitive range as already portrayed in Figure 2. Given the somewhat different localization volumes, water-signal-scaled peak areas (essentially representing molal concentrations) for the main singlets were calculated for a quantitative comparison. The following ratios of peak areas for

 Published version to be found at: https://doi.org/10.1002/mrm.28322

2DI-CSE and 3D I-CSE, respectively, with respect to the values from PRESS were found: NAA: 87.5% and 76.8%; Cr-CH_3: 90.5% and 40.5%; Cho: 83.5% and 20%. If these values are corrected by the excitation profile from Figure 2, the estimated concentrations are close to the values found for PRESS.

3.2 In vivo measurements in human brain

In both I-CSE methods the localized spectrum is the result of an appropriate add/subtract cycle over multiple acquisitions. Figure 4 illustrates the summation procedure with representative data for single subspectra from the ISIS steps together with the resulting summed, i.e. localized spectrum. For 3D I-CSE, the 8 subspectra contain signal from the whole sensitive coil volume and the size of the signal depends on the relative proportion of volumes that are recorded with inverted or non-inverted magnetization. For VOIs that are considerably smaller than the whole head, the signal from the VOI is thus much smaller than the signal in individual traces. In contrast, in 2D I-CSE the final signal from the VOI is of similar magnitude as for the subspectra since they all only contain signal from a single slice and in the illustrated example the VOI covers a substantial fraction (~50%) of that slice.

To demonstrate spectral quality in single subjects, a comparison of non-water-suppressed downfield I-CSE and MC-semi-LASER spectra is presented in Figure 5. Well resolved spectra with good SNR are obtained with all three techniques. Both, 2D I-CSE and 3D I-CSE spectra show considerably larger signals at ~8.2 ppm (attributed to exchange-affected amide signals) than for MC-semi-LASER. Further expected differences between the spectra arise from the differing excitation profiles, which are given as shaded area in the two I-CSE spectra.

Figure 6 demonstrates upfield 2D I-CSE spectra, also obtained with and without WS. Spectral quality is quite acceptable and indicates that the proffered techniques could also be used to acquire very short TE spectra from the conventional upfield region, though maybe not as robustly as with conventional techniques. The spectrum obtained with WS shows reduced baseline contributions from residual water, but quantification would be possible without this module. The difference spectrum for the acquisitions without and with WS are largely featureless, which speaks in favor of the reproducibility of the 2D technique, but also shows that the CHESS module used does not evoke large MT in the upfield region, where an MT effect is primarily expected for the creatine resonances (37).

Focusing on the main target for the novel techniques, Figure 7 shows averaged downfield spectra from 4 subjects obtained with 2D I-CSE and MC-semi-LASER; both recorded without and with

 Published version to be found at: https://doi.org/10.1002/mrm.28322

WS. Comparing the spectra without WS, difference signals are particularly prominent at 7.5-9 ppm, while the principle peak pattern and the intensities are similar at 6.5-7.5 ppm. The spectra obtained with WS have more similarities. The differences can be largely explained by the stronger T_2-weighting for semi-LASER and the limited excitation profile for I-CSE. The difference spectra reflecting signal from exchangeable protons clearly document that with the novel sequence a large fraction of those contributions can be retained, while with MC semi-LASER at an intermediate TE the effect of MT from saturated water is also clearly documented but a much smaller part of the exchangeable proton signal is retained even though the water signal is not pre-saturated.

Finally, Figure 8 serves to further define the downfield spectrum obtained with 2D I-CSE and to document the intersubject reproducibility of its features. On the left, the averaged spectrum from 8 volunteers is presented, both with and without preceding CHESS WS, as well as their difference. With the high SNR in this average spectrum, further details, particularly in the difference, can be noted. The amide signals between 7.6 and 8.6 ppm are very prominent. Equally, the 6.8ppm peak also shows a large MT effect. Furthermore, the difference spectrum highlights smaller features, in particular at 7.5, 6.3, 6.1, and 5.8 ppm. The inter-subject reproducibility can be judged when comparing the individual nWS spectra of the 8 subjects. Even the smaller features mentioned above appear to be reproduced in virtually all cases.

Discussion

In this work, two novel non-water-excitation sequences—3D I-CSE and 2D I-CSE—have been introduced that can be used on clinical scanners of 3 T or at UHF. Both are based on ISIS localization with GOIA inversion pulses followed by chemical-shift-selective excitation modules. One of them uses a slice-selective refocusing pulse to restrain ISIS localization to two dimensions. In the current work, the methods were optimized for downfield signals of exchangeable protons.

When targeting signals from exchangeable protons in the downfield region of the ^{1}H MR spectrum, one of two strategies is usually followed. i) Most widespread is indirect detection via chemical exchange-dependent saturation transfer (CEST) (38-40), which is based on saturation transfer from metabolites to water protons leading to a decrease in the water signal that depends on the irradiation frequency. It boosts sensitivity compared to direct detection by orders of magnitude, but has limits in its interpretation since multiple factors influence response intensity and in addition the spectral resolution

is limited. ii) Direct detection with MRS techniques has been adapted for observation of exchangeable protons. As mentioned in the Introduction, optimal detection sensitivity is achieved by elimination of water presaturation elements, minimization of TE, and indirectly by use of UHF scanners. Restricting the discussion to techniques that have been used successfully in vivo for human investigations, MC methods are most widespread. At 3 T, MacMillan et al. (12) have investigated the downfield spectrum and its exchange and relaxation characteristics with MC-PRESS, which limited the minimum TE to 20 ms, included a short inversion recovery period before excitation and was further limited by the duration of the inversion pulse (22 ms). At 9.4 T, the MC method was combined in human brain with STEAM (16,17) and semi-LASER (17) to elucidate the downfield spectrum. STEAM with its intrinsic 2-fold signal loss allowed to reach a TE of 8 ms (13 ms in (16)), but included a longish TM period (~50 ms), with mixing of magnetization between metabolites and water. The semi-LASER implementation had the disadvantages of longer TE (24 ms in (17)) and the ill-defined influence of the MC pre-pulse. Thus, the presently suggested ISIS-based methods are clearly advantageous, since in the current implementation they allow to go <10 ms in TE and do not include another period of unequal metabolite and water magnetization pathways. The much bigger signal yield of these new techniques compared to MC-semi-LASER for amide signals is clearly documented by Fig. 7. In particular, the difference spectra illustrating how much signal is lost upon adding a preceding CHESS water saturation module show this very clearly—even if admittedly the semi-LASER technique used is not optimal in terms of TE.

The I-CSE methods belong to the so-called nWE techniques, which in contrast to nWS methods may also offer attractive consequences for the apparent longitudinal relaxation rates of exchangeable protons. If the exchange process is faster than the inherent T_1 of the metabolite proton, longitudinal relaxation will occur faster than with this T_1 because magnetization will be recovered more efficiently by proton exchange from water if the water magnetization was left at equilibrium when the exchangeable proton was localized and detected. Thus, the T_1s of fast exchanging protons largely reflect the exchange rate for nWE methods while they can be strongly linked to the T_1 of water in general nWS methods where the longitudinal magnetization is not maintained throughout the experiment. Therefore, nWE methods were called relaxation enhancement (RE) techniques by Shemesh et al. (13,26,27) who have introduced this concept in vitro and for animal studies at UHF. They reported up to a threefold increase in the apparent longitudinal relaxation rate (27) for downfield resonances. So far, the LRE effect has been verified only at B_0 fields ≥ 9.4 T, but nWE methods have been applied to avoid signal attenuation also at 7 T, mostly for the observation of NAD^+ resonances. Except for a preliminary report (5), nWE methods have not previously been used at ≤3 T.

Even though there is no significant period of longitudinal magnetization exchange for the new methods that affects the intensity of downfield metabolite signals, proton exchange still does impact these metabolite signals during TE after selective creation of transverse magnetization for metabolites only. Therefore, minimizing TE is crucial for the observation of fast exchanging moieties. The TEs achieved in fresh mouse brains at 9.4 T (13) and rat brains in vivo at 21.1 T (26) were rather long—40 ms with a non-localized spin echo and 187 ms with 3D-LASER localization. 3D-LASER sequences require 3 pairs of adiabatic refocusing pulses. This prohibits reaching short TEs on human scanners. On an 11.7T animal scanner a TE of 14 ms was obtained for 3D-LASER (23). For human studies at lower B_0, maximum achievable B_1^+ amplitudes are much lower and frequency-selective pulses longer. Instead, to obtain a short TE of 18 ms at 7 T, 1D-LASER was used to localize a whole slice (24). A similar TE was achieved for 7 T with a 3D-localizing triple-echo sequence with optimized Shinnar-Le Roux refocusing pulses (25). The nWE method with the shortest reported TE so far was suggested by Gonçalves et al. (28) for use in rat brain at 9.4 T. It was similar to our 3D I-CSE method, first reported at about the same time in Ref (41). ISIS is a non-echo method. This makes very short TEs possible, though all full reports so far used it with spin-echo detection and TEs of 5-10 ms; only Ref. (5) had suggested direct excitation with a 1331 binomial pulse.

Both currently presented I-CSE techniques suffer from challenges posed by the ISIS technique in general and when applied to ^{1}H-MRS, in particular. One known issue with ISIS is the SAR burden of traditional adiabatic pulses, which has been addressed in this work by the use of GOIA pulses. An additional problem is so-called 'T_1-smearing', which may lead to incomplete outer volume signal cancellation for short TR. This is probably not a big issue for the downfield signals and given the minimal excitation outside the downfield range also not an issue there. In addition, extended ISIS-cycle schemes (42) could be used. The main issue with ISIS probably arises from signal instabilities, either due to small hardware fluctuations, but mostly from small physiologic or bulk subject motion that creates problems for outer volume signal cancellation. This can be addressed in three ways: (i) single scan data can be stored that allows to realign data suffering from small frequency and phase variation (realized here only in part, when we stored raw data instead of scanner-processed data); (ii) spectra to be compared later-on can be acquired in an interleaved mode; (iii) OVS pulses can be added to reduce effects of outer volume ripples in ISIS localization pulses; and (iv) as proposed with 2D I-CSE, it is possible turn to 2D-ISIS localization combined with slice-selective refocusing that includes only signal from a single slice where signal cancellation over the ISIS cycle has to work sufficiently, rather than for the whole head signal in the 3D case.

The assignment of downfield signals has been addressed by different techniques at multiple field strength, but remains difficult and unsolved. Metabolites with resonances expected in the downfield range (see discussion in (16)) include NAA, homo-carnosine (homoCs), glutamine (Gln), glutathione (GSH), adenosine-triphosphate (ATP), NAD^+, glucose (Glc), urea, phosphocreatine (PCr), low concentration aromatic compounds and in addition signals for very fast exchanging moieties (e.g., glutamate (Glu), Glc, and creatine (Cr)/PCr). In this respect, it is of interest to compare our results with previous data for humans at 3 T (12), 7 T (43) and 9.4 T (16), but also for rat brain obtained with a similar technique at 9.4 T (28).

The spectra acquired in this study are in general agreement with those presented by MacMillan et al. (12) for the same field strength. In particular, the spectra obtained with WS look quite similar. However, with the current methodology the additional resonance signals obtained without this presaturation are much larger, especially at 6.8 ppm and from 7.5-9 ppm. A similar statement can be made for a comparison to the MC-STEAM spectra obtained at 9.4 T, where again the major exchange-affected resonances are less prominent than in the current results. Other differences with respect to the nWS 9.4T spectra (16) concern the 7.8 ppm resonance (mostly NAA), which is much broader at low field. Also, the peaks further upfield (at 5.8, 6.1 and 6.3 ppm) are much less prominent in the I-CSE spectra-though that is likely just due to the excitation profile and possibly also an effect of artifacts arising from imperfect water cancellation in MC and residual water excitation with I-CSE. However, the nWS spectrum from the literature that is most comparable with ours is the one from rat brain also obtained with an ISIS technique (28). In this case, the 8.1-8.5 ppm peaks are as prominent in comparison to the 7.8 ppm peak as in the nWS I-CSE spectrum in Figure 8. The main differences to these 9.4T spectra are peak widths for the 7.8ppm peak (explained by J-splitting and a short T_2 (16) that translates to a wider peak at low field if T_2s are similar) and the 6.8ppm peak (possibly due to exchange broadening that is more prominent at lower field) on one hand and some peak heights on the other. In particular, the 6.8ppm peak and a resonance at 7.5 ppm are more prominent at 9.4 T. This would in both cases also be consistent with exchange-broadening, which may render the 7.5ppm resonance almost undetectable at 3 T if exchange rates are faster for this peak than for the 6.8ppm resonance. At 9.4 T, the linewidth is indeed larger for this peak than for the one at 6.8 ppm. The 7.5ppm peak is very prominent in the rat spectra at 9.4 T and has not been detected in any of the MC spectra before, but it is discernible, though just faintly, also in our human spectra at 3 T (most evident in the difference spectrum in Figure 8).

 Published version to be found at: https://doi.org/10.1002/mrm.28322

The largest effect of WS as evident in the difference spectrum in Figure 8 is likely due to multiple amide resonances (7.8- 8.5 ppm), known to undergo moderately fast exchange. However, ATP is also known to feature resonances at 6.1, 6.8, 8.2 and 8.5 ppm, which are suspected to be affected by MT (Overhauser effect (44)). Alternatively, GSH has also been reported to feature two resonances in the amide region (8.27 and 8.48 ppm) (45). Another potential source for the 6.8ppm peak and the 7.5ppm resonance, in particular with the evidence of fairly fast exchange, could be glutamine, which has two fast-exchanging amide protons reported to resonate at those chemical shifts (46). The peak at 5.8 ppm has been assigned to urea (16) and was also observed at 9.4 T with MC-STEAM. It had not been mentioned in Ref (12) but is discernible in some of the figures in that paper.

The presented methods and their evaluations clearly have limitations in general and also the current performance of the I-CSE techniques can be further improved in multiple ways. The main general constraint is that I-CSE techniques do not provide single-shot localization. They rely on signal cancellation from 4 or 8 subsequent acquisitions and are thus inherently sensitive to motion and instabilities, even though multiple counter-measures can be implemented to minimize the effects (see above). Two main issues of the current implementations are: (i) The currently used sinc-Gauss frequency-selective excitation pulse does not excite the entire target range and stopband ripples lead to spurious excitation of water. Numerically optimized pulses would be better. Increasing the pulse bandwidth is particularly necessary for 3D I-CSE with the selective spin-echo excitation. The use of self-refocusing pulses (47-50) would lead to shorter TEs and further minimized effects of exchange. Dual-band pulses would allow simultaneous acquisition of both down- and upfield parts of the spectrum. (ii) The volume-selection pulses have not been fully evaluated in terms of their exact localization profile, which prevented a true 1:1 comparison with PRESS or the MC techniques. Furthermore, the current study lacks quantitative evaluation of the recorded spectra, which is difficult though since fitting models for the downfield spectral region can only be heuristic in nature at present, given the lack of unequivocal assignments. Hence, even the comparison of spectra with and without water signal presaturation was only performed with difference spectra that are easier to interpret than peak area information for a complicated fit model.

 Published version to be found at: https://doi.org/10.1002/mrm.28322

Conclusions

Novel nWE sequences have been introduced that can be used at clinical field strengths and offer substantial benefits for the detection of metabolite signals that are otherwise suppressed by saturation transfer from water in standard MRS sequences. They also provide better sensitivity for moderate or fast exchanging resonances than MC techniques. Given the fact that they do not excite the water resonance, they can also be extended for the use as relaxation enhancement methods, though that will need special consideration of the effects of the magnetization inversion pulses in the localization modules. Avoiding water saturation and the option to use very short TEs allows direct observation of faster exchanging moieties than was previously possible and on top turns the methods less susceptible to fast T_2 relaxation.

Acknowledgement

This work was supported by the Swiss National Science Foundation (320030-175984).

 Published version to be found at: https://doi.org/10.1002/mrm.28322

References

1. Haase A, Frahm J, Hanicke W, Matthaei D. 1H NMR chemical shift selective (CHESS) imaging. Phys Med Biol 1985;30(4):341-344.
2. Keller PJ, Hunter WW, Jr., Schmalbrock P. Multisection fat-water imaging with chemical shift selective presaturation. Radiology 1987;164(2):539-541.
3. Tkac I, Starcuk Z, Choi IY, Gruetter R. In vivo 1H NMR spectroscopy of rat brain at 1 ms echo time. Magn Reson Med 1999;41(4):649-656.
4. Dong Z. Proton MRS and MRSI of the brain without water suppression. Prog Nucl Magn Reson Spectrosc 2015;86–87:65-79.
5. Kreis R, Boesch C. Localized 1H-MRS without water saturation: Techniques and initial results for human brain and muscle. In Proceedings of the 6th Annual Meeting of ISMRM, Sydney, Australia, 1998. p 24.
6. Hurd RE, Gurr D, Sailasuta N. Proton spectroscopy without water suppression: the oversampled J- resolved experiment. Magn Reson Med 1998;40:343-347.
7. Nixon TW, McIntyre S, Rothman DL, De Graaf RA. Compensation of gradient-induced magnetic field perturbations. J Magn Reson 2008;192(2):209-217.
8. Mori S, Eleff SM, Pilatus U, Mori N, van Zijl PC. Proton NMR spectroscopy of solvent-saturable resonances: a new approach to study pH effects in situ. Magn Reson Med 1998;40:36-42.
9. Piotto M, Saudek V, Sklenar V. Gradient-tailored excitation for single-quantum NMR spectroscopy of aqueous solutions. J Biomol NMR 1992;2:661-665.
10. Dreher W, Leibfritz D. New method for the simultaneous detection of metabolites and water in localized in vivo 1H nuclear magnetic resonance spectroscopy. Magn Reson Med 2005;54(1):190-195.
11. De Graaf RA, Sacolick LI, Rothman DL. Water and metabolite-modulated MR spectroscopy and spectroscopic imaging. In Proceedings of the 14th Annual Meeting of ISMRM. Seattle, Washington, USA, 2006. p 3063
12. MacMillan EL, Chong DGQ, Dreher W, Henning A, Boesch C, Kreis R. Magnetization exchange with water and T1 relaxation of the downfield resonances in human brain spectra at 3.0 T. Magn Reson Med 2011;65:1239-1246.
13. Shemesh N, Dumez JN, Frydman L. Longitudinal relaxation enhancement in 1H NMR spectroscopy of tissue metabolites via spectrally selective excitation. Chemistry 2013;19:13002-13008.
14. MacMillan EL, Boesch C, Kreis R. Magnetization exchange observed in human skeletal muscle by non-water-suppressed proton MR spectroscopy. Magn Reson Med 2013;70:916-924.
15. Hock A, MacMillan EL, Fuchs A, Kreis R, Boesiger P, Kollias SS, Henning A. Non-water-suppressed proton MR spectroscopy improves spectral quality in the human spinal cord. Magn Reson Med 2013;69:1253-1260.
16. Fichtner ND, Giapitzakis IA, Avdievich N, Mekle R, Zaldivar D, Henning A, Kreis R. In vivo characterization of the downfield part of 1H MR spectra of human brain at 9.4 T: Magnetization exchange with water and relation to conventionally determined metabolite content. Magn Reson Med 2017;79:2863-2873.
17. Giapitzakis IA, Shao T, Avdievich N, Mekle R, Kreis R, Henning A. Metabolite-cycled STEAM and semi-LASER localization for MR spectroscopy of the human brain at 9.4T. Magn Reson Med 2018;79:1841-1850.

18. Emir UE, Burns B, Chiew M, Jezzard P, Thomas MA. Non-water-suppressed short-echo-time magnetic resonance spectroscopic imaging using a concentric ring k-space trajectory. NMR Biomed 2017;30:e3714.
19. Döring A, Adalid V, Boesch C, Kreis R. Diffusion–weighted magnetic resonance spectroscopy boosted by simultaneously acquired water reference signals. Magn Reson Med 2018;80(6):2326-2338.
20. Döring A, Kreis R. Magnetic resonance spectroscopy extended by oscillating diffusion gradients: Cell-specific anomalous diffusion as a probe for tissue microstructure in human brain. Neuroimage 2019;202:116075.
21. Bottomley PA; General Electric Company, assignee. Selective volume method for performing localized NMR spectroscopy. U.S. patent 4,480,228. 1984.
22. Ordidge RJ, Connelly A, Lohmann JAB. Image-selected in vivo spectroscopy (ISIS). A new technique for spatially selective NMR spectroscopy. J Magn Reson 1986;66:283-294.
23. de Graaf RA, Behar KL. Detection of cerebral NAD+ by in vivo 1H NMR spectroscopy. NMR Biomed 2014;27:802-809.
24. De Graaf RA, De Feyter HM, Brown PB, Nixon TW, Rothman DL, Behar KL. Detection of cerebral NAD+ in humans at 7T. Magn Reson Med 2016;32:828-835.
25. Bagga P, Hariharan H, Wilson NE, Beer JC, Shinohara RT, Elliott MA, Baur JA, Marincola FM, Witschey WR, Haris M, Detre JA, Reddy R. Single-Voxel (1) H MR spectroscopy of cerebral nicotinamide adenine dinucleotide (NAD(+)) in humans at 7T using a 32-channel volume coil. Magn Reson Med 2020;83(3):806-814.
26. Rosenberg JT, Shemesh N, Muniz JA, Dumez JN, Frydman L, Grant SC. Transverse relaxation of selectively excited metabolites in stroke at 21.1T. Magn Reson Med 2017;77:520-528.
27. Shemesh N, Rosenberg JT, Dumez JN, Muniz JA, Grant SC, Frydman L. Metabolic properties in stroked rats revealed by relaxation-enhanced magnetic resonance spectroscopy at ultrahigh fields. Nat Commun 2014;5:4958.
28. Gonçalves SI, Ligneul C, Shemesh N. Short echo time relaxation-enhanced MR spectroscopy reveals broad downfield resonances. Magn Reson Med 2019;82(4):1266-1277.
29. Connelly A, Counsell C, Lohman JAB, Ordidge RJ. Outer volume suppressed image related in vivo spectroscopy (OSIRIS), a high-sensitivity localization technique. J Magn Reson 1988;78:519-525.
30. Mlynárik V, Gambarota G, Frenkel H, Gruetter R. Localized short-echo-time proton MR spectroscopy with full signal-intensity acquisition. Magn Reson Med 2006;56(5):965-970.
31. Tannus A, Garwood M. Adiabatic pulses. NMR Biomed 1997;10:423-434.
32. Bogner W, Chmelik M, Andronesi OC, Sorensen AG, Trattnig S, Gruber S. In vivo 31P spectroscopy by fully adiabatic extended image selected in vivo spectroscopy: a comparison between 3 T and 7 T. Magn Reson Med 2011;66(4):923-930.
33. Andronesi OC, Ramadan S, Ratai E-M, Jennings D, Mountford CE, Sorensen AG. Spectroscopic imaging with improved gradient modulated constant adiabaticity pulses on high-field clinical scanners. J Magn Reson 2010;203(2):283-293.
34. Mao J, Mareci TH, Scott KN, Andrew ER. Selective inversion radiofrequency pulses by optimal control. J Magn Reson 1986;70:310-318.
35. Ogg RJ, Kingsley PB, Taylor JS. WET, a T1- and B1-insensitive water-suppression method for in vivo localized 1H NMR spectroscopy. J Magn Reson 1994;104(1):1-10.
36. Naressi A, Couturier C, Devos JM, Janssen M, Mangeat C, de Beer R, Graveron-Demilly D. Java-based graphical user interface for the MRUI quantitation package. MAGMA 2001;12(2-3):141-152.

37. Kruiskamp MJ, de Graaf RA, van der Grond J, Lamerichs R, Nicolay K. Magnetic coupling between water and creatine protons in human brain and skeletal muscle, as measured using inversion transfer (1)H-MRS. NMR Biomed 2001;14(1):1-4.
38. Ward KM, Aletras AH, Balaban RS. A new class of contrast agents for MRI based on proton chemical exchange dependent saturation transfer (CEST). J Magn Reson 2000;143(1):79-87.
39. Jones CK, Schlosser MJ, van Zijl PC, Pomper MG, Golay X, Zhou J. Amide proton transfer imaging of human brain tumors at 3T. Magn Reson Med 2006;56(3):585-592.
40. van Zijl PCM, Lam WW, Xu J, Knutsson L, Stanisz GJ. Magnetization transfer contrast and chemical exchange saturation transfer MRI. Features and analysis of the field-dependent saturation spectrum. Neuroimage 2018;168:222-241.
41. Dziadosz M. BW, Döring A, Kreis R. Novel methods to record MR spectra in human brain without suppressing or exciting the water signal to investigate exchange-sensitive protons. . In Proceedings of the 27th Annual Meeting of the ISMRM, Montreal, Canada, 2019. p 46
42. Ljungberg M, Starck G, Vikhoff-Baaz B, Alpsten M, Ekholm S, Forssell-Aronsson E. Extended ISIS sequences insensitive to T(1) smearing. Magn Reson Med 2000;44(4):546-555.
43. Fichtner ND, Henning A, Zoelch N, Boesch C, Kreis R. Elucidation of the downfield spectrum of human brain at 7 T using multiple inversion recovery delays and echo times. Magn Reson Med 2017;78(1):11-19.
44. Goerke S, Zaiss M, Kunz P, Klika KD, Windschuh JD, Mogk A, Bukau B, Ladd ME, Bachert P. Signature of protein unfolding in chemical exchange saturation transfer imaging. NMR Biomed 2015;28(7):906-913.
45. Grande S, Luciani AM, Rosi A, Guidoni L, Viti V. Identification of amide protons of glutathione in MR spectra of tumour cells. NMR Biomed 2008;21(10):1057-1065.
46. Khlebnikov V, van der Kemp WJM, Hoogduin H, Klomp DWJ, Prompers JJ. Analysis of chemical exchange saturation transfer contributions from brain metabolites to the Z-spectra at various field strengths and pH. Sci Rep 2019;9(1):1089.
47. Geen H. FR. Band-selective radiofrequency pulses. J Magn Reson 1991;93(1):93-141.
48. Freeman R. Shaped radiofrequency pulses in high resolution NMR. Prog Nucl Magn Reson Spectrosc 1998;32(1):59-106.
49. Maudsley A, Matson G. Selective excitation in MRI and MR spectroscopy Encyclopedia of Magnetic Resonance John Wiley & Sons, Ltd, 2007. doi:10.1002/9780470034590.emrstm0483.
50. Morris. PG. Complex radiofrequency pulses. Encyclopedia of Magnetic Resonance: John Wiley & Sons, Ltd, 2007. doi.org/10.1002/9780470034590.emrstm0085.

Figure captions

Figure 1

Sequence diagrams of the proposed non-water-excitation (nWE) MRS methods.

Upper row: Three-dimensional **I**SIS localization with **C**hemical-**S**hift-Selective **E**xcitation termed **3D I-CSE**. ***Lower row:*** Two-dimensional **I**SIS localization with **C**hemical-**S**hift-Selective **E**xcitation and slice-selective spin echo, termed **2D I-CSE**. Both sequences contain an ISIS element for localization implemented with adiabatic GOIA-WURST inversion pulses and frequency-selective excitation targeting metabolite resonances while leaving water magnetization untouched. In 2D I-CSE, one direction is localized by a slice-selective refocusing pulse instead of a third ISIS element. Optional elements preceding localization and excitation include OVS and water presaturation pulses that can be interleaved.

ISIS localization is the result of an add/subtract scheme for different scans where the adiabatic inversion pulses are played out in different combinations. The applied combination of pulses and corresponding add/subtract scheme for the receiver (ADC) are listed in the Tables to the right of the diagrams.

Figure 2

Illustration of the excitation pulse profiles for 2D I-CSE (A) and 3D I-CSE (B).

The presented frequency responses were obtained from 41 phantom measurements with varying frequency offsets for the applied pulses (from -10.0 to +10.0 ppm in 0.5 ppm steps). The responses were frequency-shifted, summed and broadened in jMRUI for display.

Figure 3

Illustration of the in vitro performance of the I-CSE techniques in comparison to standard PRESS.

^{1}H MRS spectra for the upfield region in a “braino” phantom were obtained with **PRESS** (top), **2D I-CSE** (middle) and **3D I-CSE** (bottom).

I-CSE spectra were recorded using an offset of -4 ppm with respect to the water peak. The spectra have been apodized by 2 Hz for display and are plotted as scaled by the area of the water signal recorded in separate scans with on-resonance excitation. Intensity differences thus mostly reflect the excitation profile of the I-CSE techniques.

Figure 4

Illustration of the localization process through the add/subtract procedure of single acquisitions with different preinversion pulses applied as needed for the ISIS techniques.

Spectra from individual ISIS steps (each spectrum in turn representing an average over 2 acquisitions for 3D I-CSE and 4 for 2D I-CSE, respectively) that contain signal from the whole sensitive volume (3D I-CSE,

 Published version to be found at: https://doi.org/10.1002/mrm.28322

on the right) or a slice only (2D I-CSE, on the left) are displayed together with the summed signal representing the resulting localized spectrum (bottom traces).

In vivo data from a single healthy subject, 3 Hz apodization applied for display purposes. For 3D I-CSE, the individual ISIS step spectra are displayed with a scaling factor of 1/10 compared to the sum spectrum.

Figure 5

Illustration of the in vivo performance of the I-CSE techniques for the downfield spectral region in comparison to MC-semi-LASER.

Comparison of downfield in-vivo brain spectra acquired from a supraventricular VOI in a single subject with **2D I-CSE** (left), **3D I-CSE** (middle) and **MC-semi-LASER** (right column) All spectra were recorded without water presaturation with equal acquisition time and equal shim settings. The approximated excitation profiles are overlaid in color for the I-CSE techniques. The spectra were scaled by the area of the water signal recorded in separate scans with on-resonance excitation.

(Excitation pulses were centered at 9.7 ppm for 2D I-CSE and 8.7 ppm for 3D I-CSE; 128 acquisitions each, 3000 ms TR, 3 Hz Gaussian line broadening).

Figure 6

Illustration of the in vivo performance of the 2D I-CSE technique for the standard upfield spectral region in a single subject and demonstration of the effect of water presaturation in a spectral region where only small MT effects are expected.

Representative upfield spectra acquired with 2D I-CSE from a supraventricular VOI (20x40x20 mm^3) in a single subject without (top, solid line) and with (middle, dashed line) water presaturation. The difference spectrum at the bottom contains only minor spectral features, some of them reflection of signal instability (dispersive signals for the large NAA and choline peaks) rather than true MT effects (most reproducible for the creatine methyl peak).

Figure 7

Illustration of downfield spectra acquired with a nWE and a MC technique and of the MT effect for a water-presaturation module for both methods.

^{1}H MR spectra acquired with 2D I-CSE (TE 10.2 ms, left in red) and MC-semi-LASER (TE 35 ms, right in green) from a large supraventricular VOI of 65 cm^3. **Top, solid line**: spectra acquired without water presaturation. **Middle, dashed line:** spectra with the CHESS module. **Bottom, gray line:** difference of nWS minus WS spectra. The spectra represent averages over the same four subjects for both methods, with acquisition settings kept identical. Spectra were not scaled. Quite obviously, there are substantial differences for the spectra from the two techniques, both for the cases with (mostly effects of TE) and without (additional effects of fast exchange) WS, where TE effects are prominent for the NAA amide

peak at 7.8 ppm with short T_2 and where exchange effects are particularly strong at 8.2 ppm for exchangeable amide protons.

(To calculate the difference signal, zero filling was applied, followed by frequency alignment in frequency domain and truncation to the original number of points, followed by apodization with 3 Hz Gaussian line broadening.)

Figure 8.

Illustration of the main cohort results for the downfield spectrum as obtained with the 2D I-CSE method.

The cohort average spectrum for 8 healthy subjects as obtained from a supraventricular mixed GM/WM VOI is displayed on the left and the individual spectra on the right.

The solid red line represents the average spectrum obtained without WS, while the red dashed line corresponds to the same experiment preceded by WS. The difference (nWS – WS) is presented as a solid gray line at the bottom, where peaks that are mentioned in the text are indicated by arrows and labeled by their chemical shift. The individual spectra on the right illustrate the stability of the introduced technique and the reproducibility of most small spectral features with uncertain assignments.

(Excitation at 9.7 ppm, 128 acquisitions per spectrum per subject, 3 Hz Gaussian line broadening, no interindividual scaling applied)

 Published version to be found at: https://doi.org/10.1002/mrm.28322

3D I-CSE

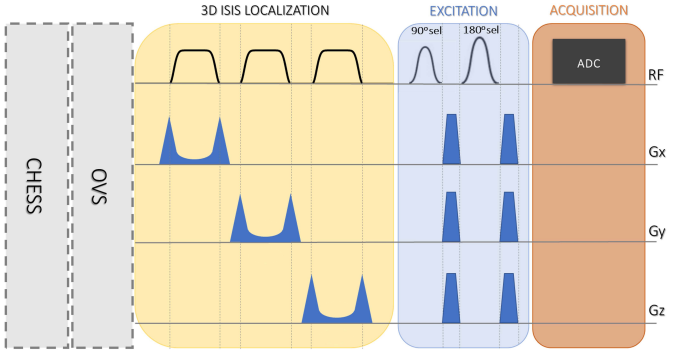

2D I-CSE

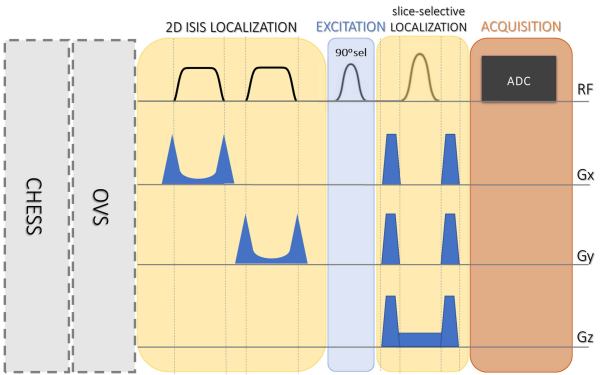

Figure 1

ISIS step	X	Y	Z	ADC
1	OFF	OFF	OFF	+
2	ON	**ON**	**ON**	-
3	**ON**	OFF	**ON**	+
4	OFF	OFF	**ON**	-
5	**ON**	**ON**	OFF	+
6	**ON**	OFF	OFF	-
7	OFF	**ON**	**ON**	+
8	OFF	**ON**	OFF	-

ISIS step	X	Y	Z	ADC
1		**ON**	**ON**	+
2		**ON**	OFF	-
3		OFF	**ON**	-
4		OFF	OFF	+

Figure 2

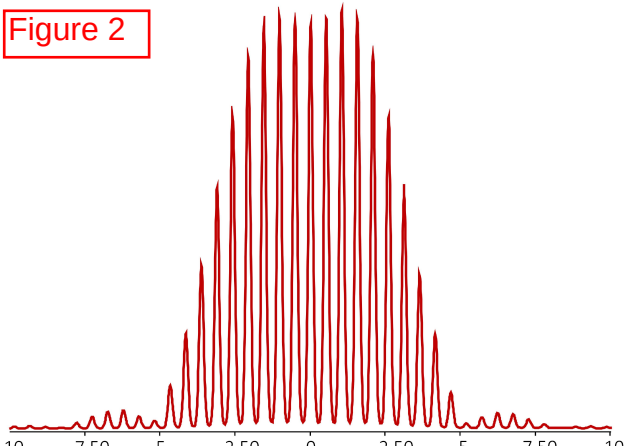
10
7.50
5
2.50
0
-2.50
-5
-7.50
-10
chemical shift (ppm)

A.

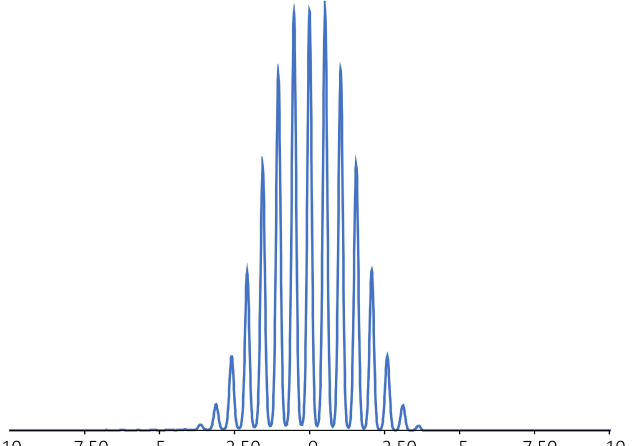
10
7.50
5
2.50
0
-2.50
-5
-7.50
-10
chemical shift (ppm)

B.

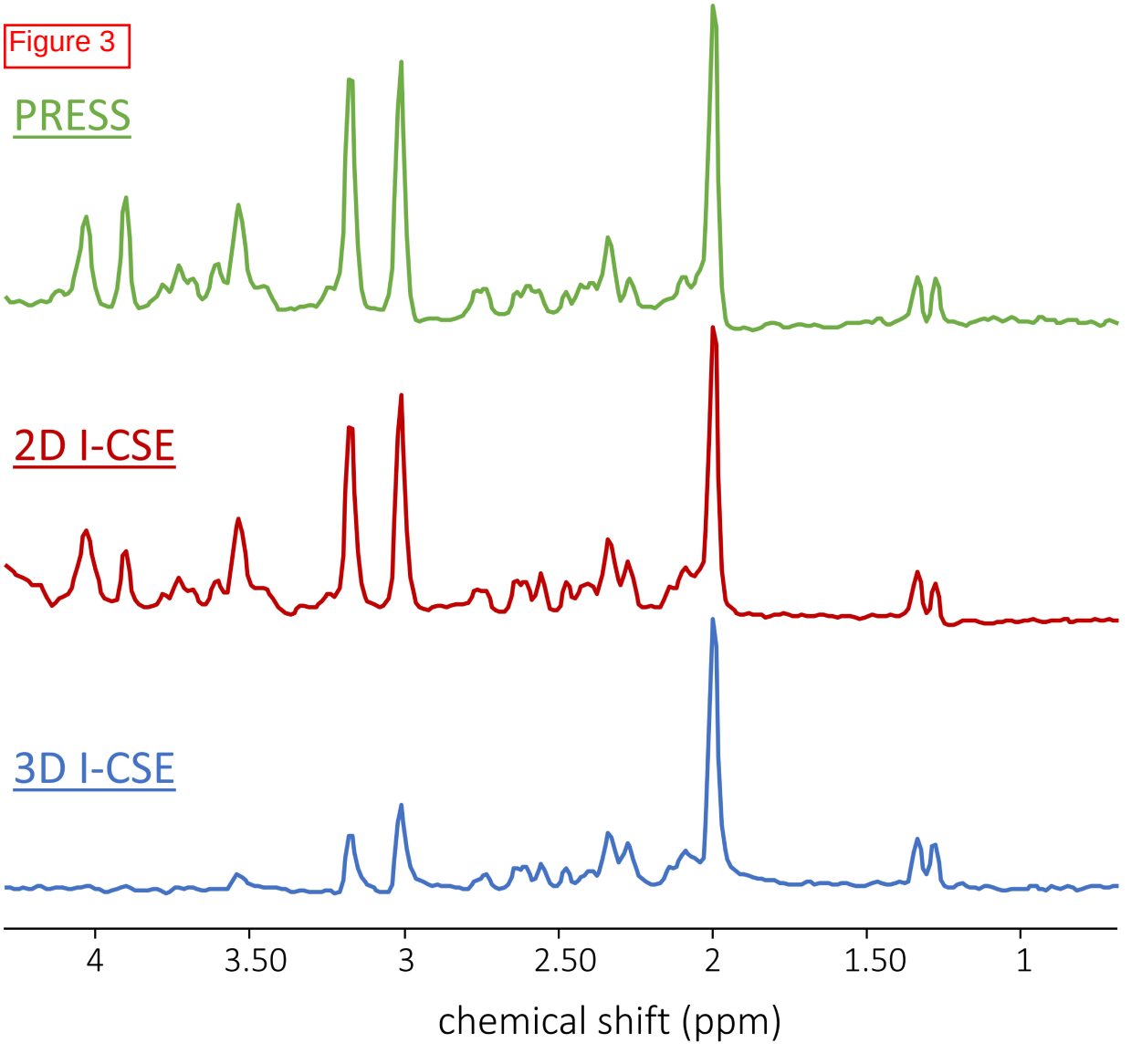
Figure 3
PRESS
2D I-CSE
3D I-CSE
4
3.50
3
2.50
2
1.50
1
chemical shift (ppm)

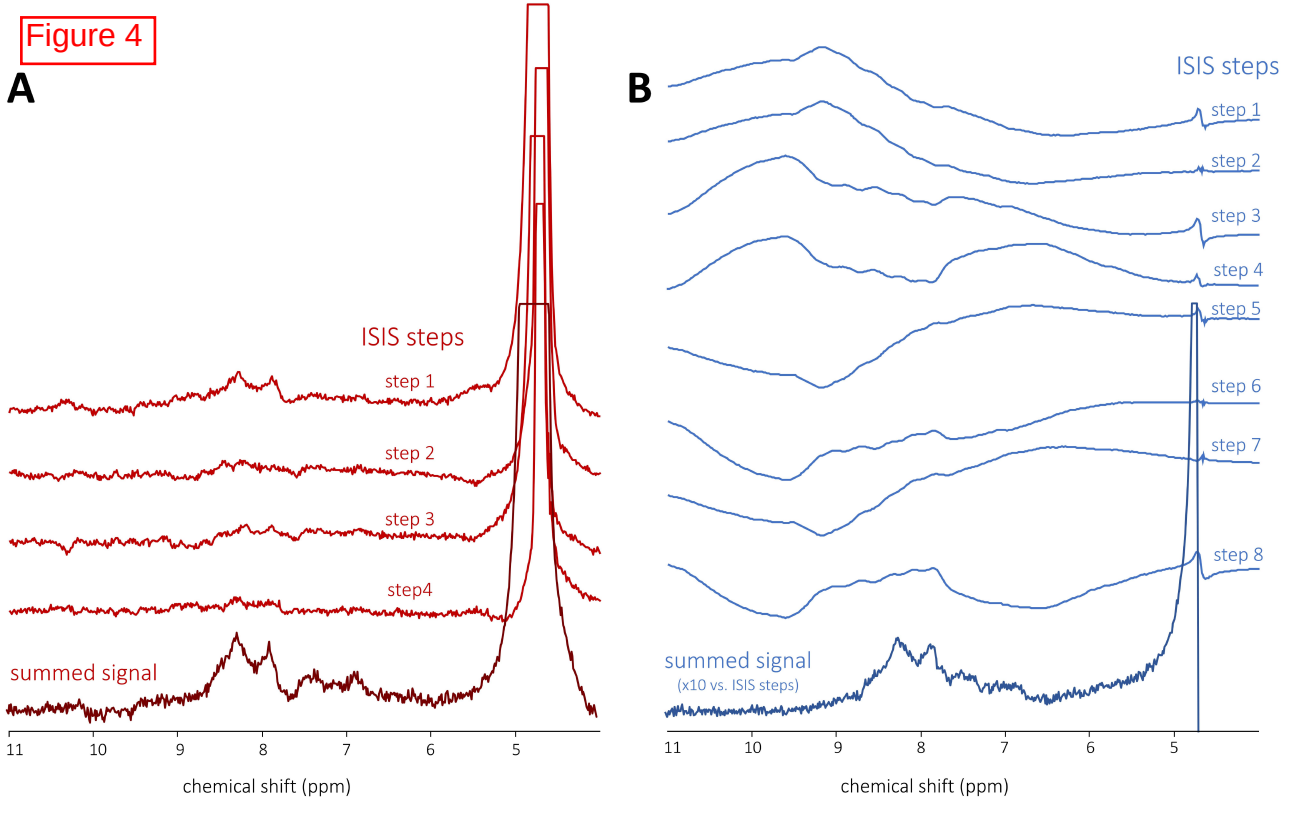
Figure 4
A
ISIS steps
step 1
step 2
step 3
step4
summed signal
11
10
9
8
7
6
5
chemical shift (ppm)
B
ISIS steps
step 1
step 2
step 3
step 4
step 5
step 6
step 7
step 8
summed signal
(x10 vs. ISIS steps)
11
10
9
8
7
6
5
chemical shift (ppm)

Figure 5

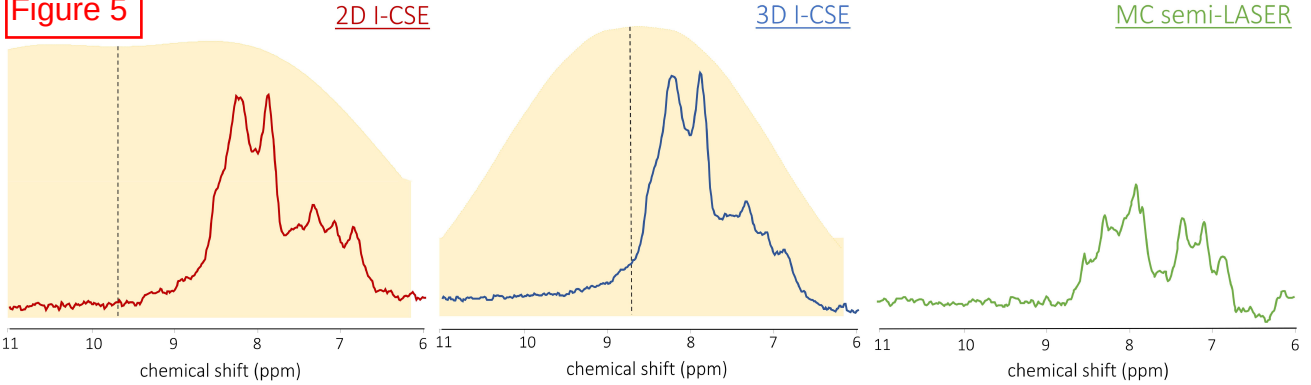

Figure 6

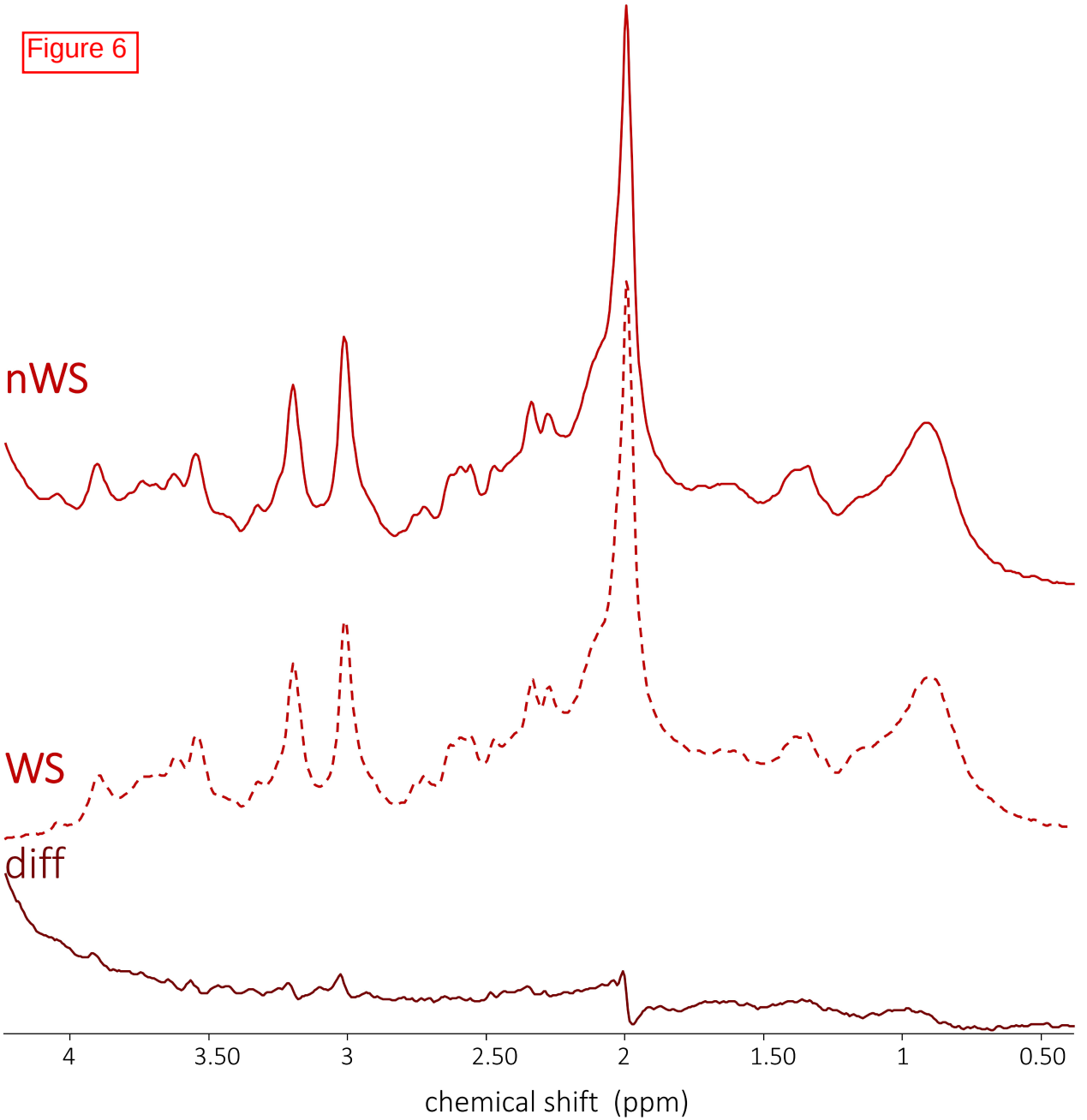

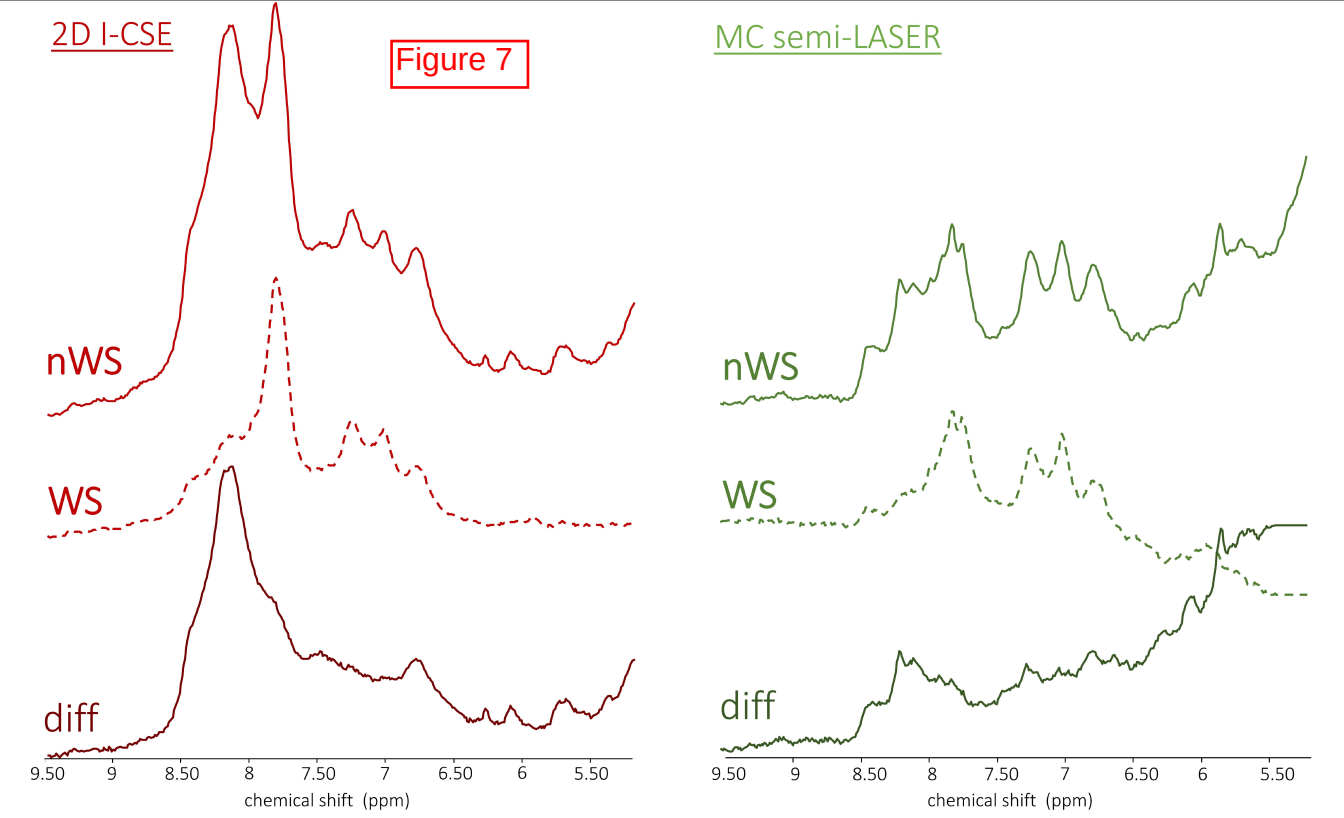
2D I-CSE
Figure 7
MC semi-LASER
nWS
WS
diff
nWS
WS
diff
9.50
9
8.50
8
7.50
7
6.50
6
5.50
chemical shift (ppm)
9.50
9
8.50
8
7.50
7
6.50
6
5.50
chemical shift (ppm)

Figure 8

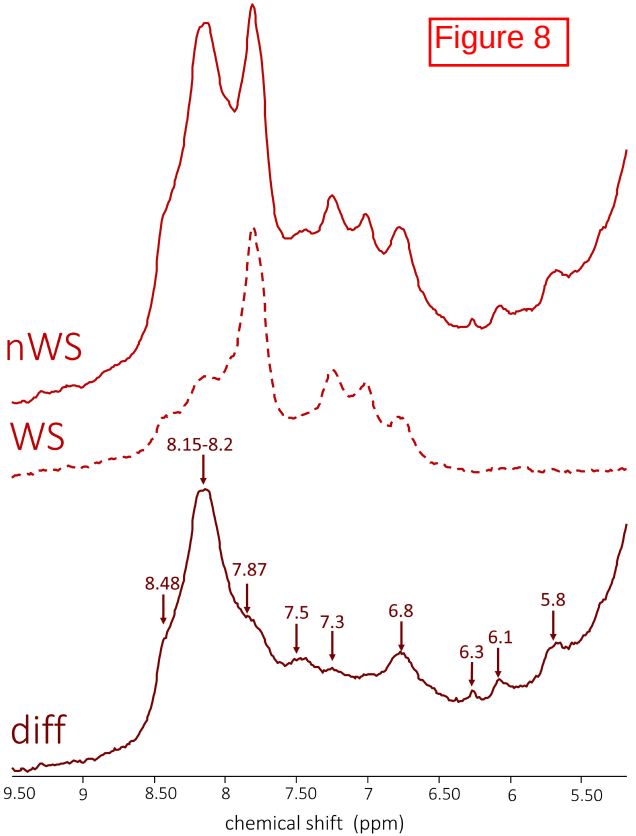
nWS
WS
8.15-8.2
8.48
7.87
7.5
7.3
6.8
6.3
6.1
5.8
diff
9.50
9
8.50
8
7.50
7
6.50
6
5.50
chemical shift (ppm)

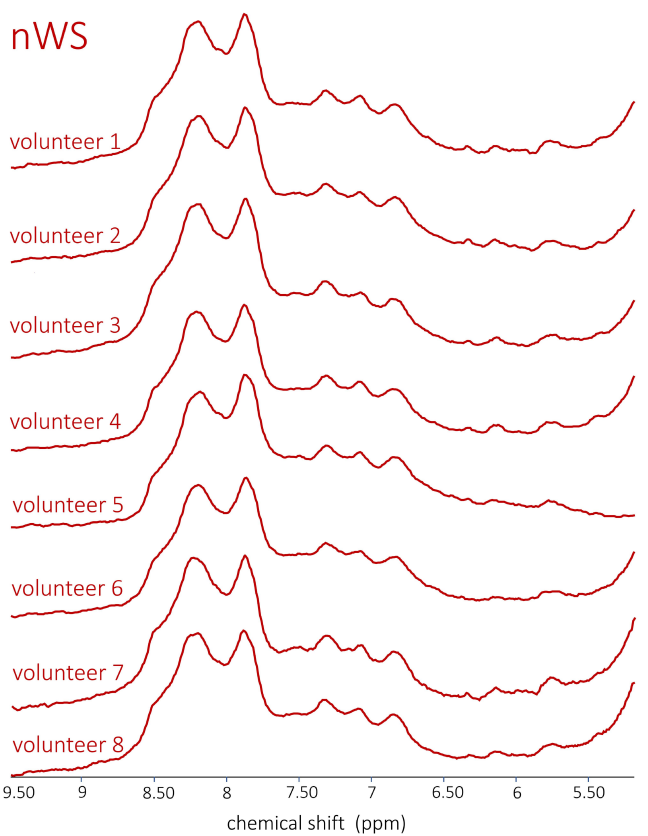
nWS
volunteer 1
volunteer 2
volunteer 3
volunteer 4
volunteer 5
volunteer 6
volunteer 7
volunteer 8
9.50
9
8.50
8
7.50
7
6.50
6
5.50
chemical shift (ppm)